Effect of kinetics on the thermal performance of a sorption heat storage reactor

M. Gaeini **(TUE)**
H.A. Zondag **(ECN)**
C.C.M. Rindt **(TUE)**

November 2016
ECN-W--16-032

Applied Thermal Engineering 102 (2016) 520–531

Contents lists available at ScienceDirect

Applied Thermal Engineering

journal homepage: www.elsevier.com/locate/apthermeng

Research Paper

Effect of kinetics on the thermal performance of a sorption heat storage reactor

M. Gaeini [a], H.A. Zondag [a,b], C.C.M. Rindt [a,*]

[a] Eindhoven University of Technology, Department of Mechanical Engineering, P.O. Box 513, 5600MB Eindhoven, The Netherlands
[b] ECN, Energy Research Center of the Netherlands, P.O. Box 1, 1755ZG Petten, The Netherlands

HIGHLIGHTS

- Mathematical model for a thermochemical heat storage system is developed.
- Kinetics model, isotherm curves and heat losses from wall are incorporated.
- Model is validated by comparing temperature profile and heat flux with experiment.
- Effect of kinetics and residence time on performance of reactor is studied.
- Full scale thermochemical heat storage reactor is optimized.

ARTICLE INFO

Article history:
Received 11 December 2015
Accepted 12 March 2016
Available online 21 March 2016

Keywords:
Sorption heat storage
Water vapor adsorption on 13X
Transfer phenomena in fixed bed reactor
Kinetics and equilibrium
Energy flows
Residence time

ABSTRACT

To reach high solar fractions for solar thermal energy in the built environment, long-term heat storage is required to overcome the seasonal mismatch. A promising method for long term heat storage is to use thermochemical materials, TCMs. In this research, a lab-scale test thermochemical heat storage system is tested experimentally and modeled numerically. Water-zeolite 13X is used as the working pair in an open packed bed reactor. The purpose of this study is to understand the effects of the kinetic parameters for the adsorption of water vapor on zeolite 13X (2 mm spherical beads), on the thermal performance of a sorption heat storage packed bed reactor. A mathematical model is developed incorporating the kinetics model and the isotherm curves and including the heat losses from the side wall of the reactor, and is validated by comparing the calculated temperature profiles with experimental ones from a lab-scale test setup. The numerical and experimental results are used to calculate the heat fluxes in the reactor and are compared to evaluate the thermal performance of the reactor. With the validated model, a parameter study is carried out into the effect of the reaction kinetics and the gas flow rate on thermal performance of a thermochemical heat storage reactor under full scale normal operating conditions. From this work, predictions of the thermal dynamics of an adsorption bed on reactor scale can be achieved, which can and will be used for further studies on the design and optimization of a thermochemical heat storage system.

1. Introduction

Replacing fossil fuels by solar energy is of high interest to reduce climate change and depletion of fossil fuel resources. According to the International Energy Agency (IEA), the building sector is the largest consumer of energy and accounts for approximately 40% of the world's total primary energy consumption, and 24% of the world's total CO_2 emission [1]. Therefore, significant reductions in fossil fuel consumption are possible by increasing the use of renewable energy in this sector. Solar energy is one of the most promising sustainable energy sources for replacing fossil fuels. In residential buildings use can be made of solar thermal collectors, photovoltaic panels and passive design measures. Since both the solar irradiation and the domestic heating demand show large asynchronous variations between day and night and over a year [2], heat storage is necessary to make effective use of the available solar energy. Long-term heat storage is needed to overcome the seasonal mismatch between heating demand and solar energy supply.

Thermal storage technologies suitable for building applications are classified in three methods based on the storage principle used: sensible, latent and thermochemical heat storage [3]. The later heat storage method makes use of a reversible physical or chemical

* Corresponding author.
E-mail address: C.C.M.Rindt@tue.nl (C.C.M. Rindt).

http://dx.doi.org/10.1016/j.applthermaleng.2016.03.055
1359-4311/

Nomenclature

Greek symbols

α	isotherm model parameter [–]
ϵ	porosity [–]
η	efficiency of the reactor [–]
λ	conductivity [W/m K]
μ	viscosity [Pa s]
ϕ	volumetric gas flow rate [m^3/s]
ρ	density [kg/m^3]
τ	tortuosity [–]; residence tie [s]

Other symbols

ΔE	activation energy of desorption [J/mol]
ΔH	adsorption enthalpy [J/mol]
A	cross-sectional area [m^2]
b	isotherm model affinity constant [–]
c	concentration of water [mol/m^3]
C_P	specific heat capacity [J/kg K]
D	dispersion or diffusion [m^2/s]
d	diameter [m]
k	kinetics coefficient [1/s]
L	length of the bed [m]
M	molecular mass [kg/mol]
n	isotherm model exponent constant [–]
q	water loading in solid [mol/kg]
R	heat resistance [m K/W]; gas constant [J/K mol]
T	temperature [K]
t	time [s]
u	velocity [m/s]
z	axial coordinate [m]

Subscripts

0	at reference temperature (273.15 K)
amb	ambient
b	bed
cond	conductive heat transfer
conv	convective heat transfer
eq	equilibrium
f	film
g	gas phase
i	inner
in	inlet
ins	insulation layer
LDF	Linear Driving Force
o	outer
out	outlet
P	macropore
p	particle
PM	porous media
SS	stainless steel layer
tef	Teflon layer
v	water vapor
w	wall

reaction and has higher energy storage density and almost no heat loss, compared to the two other heat storage methods [4]. Heat is stored into an endothermal dissociation reaction, splitting the thermochemical material into two components (charging), and, at a later time, the energy can be retrieved from the reverse exothermal reaction between the two components (discharging) according to the reaction $A(s) + B(g) \leftrightarrow AB(s) + heat$. An interesting storage material should be low cost, non-toxic, non-corrosive and stable with high energy storage density [5]. A candidate fulfilling these requirements is zeolite which can adsorb and desorb water vapor in an efficient and reversible way. Heat generated by a solar collector during summer can be employed to desorb water from the zeolite (at temperature range of 150–180 °C), and the energy stored in this way can be released during winter by introducing water vapor to the dehydrated zeolite. Although zeolite is too expensive (1–3 €/kg [6]) to be used in a full scale seasonal heat storage, it is still a good candidate to be used in scientific reactor studies because of its stability [7]. In this study, zeolite 13X in the form of spherical beads with an average diameter of 2 mm is used as sorbent. It is noted here that the physical phenomenon of fixation or capture of water vapor (sorbate) by zeolite (sorbent) is defined under the term sorption, however the expressions "thermochemical" and "sorption" are used differently by authors [8]. Sorption heat storages are usually also denoted as thermochemical heat storages, even though the process is not based on a chemical reaction, but on a physical ad/desorption reaction [9].

The most important part of the system which can provide such long-term heat storage for a residential building is the reactor in which the zeolite 13X reacts with water vapor taken from humidified air. In a practical real system applied in the built environment, a borehole system can be employed as the humidifier [10]. In the literature, both open and closed systems are investigated for long-term thermal storage of solar energy [11]. In an open system, both sorbate and energy are exchanged between the system and the surrounding environment, in a closed system, only energy is exchanged between the system and the surrounding environment. In this work, an open system is used, because the open system concept seems more promising because of robustness and low cost [12]. In addition, a packed bed reactor design was chosen. In spite the risk of non-uniform flow leading to non-reactive zones in the storage material in the packed bed concept [13], which can be avoided by consideration of specific measures in the design of the reactor, the packed bed reactor design is advantageous because of low need of auxiliary energy in comparison with other types of reactors such as fluidized bed or screw reactors [14]. However, in order to achieve a high efficiency in the thermochemical heat storage system, the reactor should be optimally designed for the intended reaction and operational condition. This requires an in-depth understanding of the physical process inside the reactor [15], which can be done by developing a validated numerical model.

For optimization and up-scaling from the lab-scale reactor size, a reactor model is needed to predict the thermal performance. For long term calculations of the energy provided by the thermochemical system, a simple and fast model requiring small computational power is needed. In this work, a one-dimensional reactor model considering the heat resistances in radial direction (quasi 2D) is developed, which can be used for annual performance calculations. On reactor scale, adsorption models are developed of water into zeolite 13X in closed sorption heat storage systems for various type of applications. Examples are a waste heat adsorption cooling system associated with the coupled heat and mass transfer mechanisms in the adsorbent [16], and the coupled heat and mass transfers occurring in closed storage systems for entire cycles under extreme conditions [17]. They are based on a one dimensional model first introduced in [18] for the heat pump process, and further developed into a two dimensional model in [19]. An extensive experimental and numerical investigations on the water vapor adsorption into zeolite 13X in an open system is done by Mette et al. [20]. In these reactor models, local thermodynamic

equilibrium is maintained for heat and mass transfer between the solid and gas phases.

In a more detailed reactor model, the characteristics of the sorption process can be described by a material model. In literature, several material models are developed for the water vapor adsorption into zeolite. Ahn and Lee [21] studied the effect of capillary condensation on adsorption and thermal desorption of water in zeolite 13X, by considering an elaborate model for the equilibrium amount of adsorbed water. Dawoud et al. [22] developed a non-isothermal model for adsorption of water vapor into a consolidated zeolite layer and studied the temperature dependence of the micro-pore diffusion. In all mentioned works, a Linear Driving Force (LDF) model is used as the kinetics model. The LDF-model is widely used for adsorption modeling due to its simplicity and physical consistency [23]. More comprehensive kinetic models have been developed to take account of fundamental features of solid-state reactions at a grain scale, but are quite cumbersome to handle at a continuum-scale calculation [24].

The purpose of this study is to understand the effects of the kinetic parameters for the adsorption of water vapor on zeolite 13X, on the thermal performance of a thermochemical heat storage packed bed reactor. A mathematical model is developed incorporating the kinetic model and the isotherm curves and including the heat losses from the side wall of the reactor, and is validated by comparing the calculated temperature profiles with experimental ones from a lab-scale test setup. The numerical and experimental results are used to calculate the heat fluxes in the reactor and are compared to evaluate the thermal performance of the reactor. With the validated model, a parameter study is carried out into the effect of the reaction kinetics and the gas flow rate on thermal performance of a thermochemical heat storage reactor under full scale normal operating conditions. From this work, predictions of the thermal dynamics of an adsorption bed on reactor scale can be achieved, which can be used for further studies on the design and optimization of a thermochemical heat storage system.

2. Experimental setup

A lab-scale reactor is realized to work as a sorption heat storage system, working with water vapor adsorption on zeolite 13X. The used zeolite 13X consists of spherical beads with an average diameter of 2 mm. The results from the measurements are used to validate the model. The setup can be divided into three main sections as shown in Fig. 1. The first section is where the humidity and flow rate of the airflow into the reactor are prepared in a controlled way by means of a Gas Flow Controller (GFC), a Liquid Flow Controller (LFC) and a Controlled Evaporator Mixer (CEM). For hydration, the dry air flow regulated by the GFC and the liquid water flow regulated by the LFC pass through the CEM. Liquid water is vaporized and mixed with dry air and the resulting humid air is introduced to the reactor. For dehydration, almost dry air flow regulated by the GFC passes through a heater and the heated air goes to the reactor.

The second section, the reactor, is the main part of the setup. The volume of the reactor is 0.42 l and is filled with 317 g of zeolite 13X beads placed on top of a filter at the bottom of the reactor. The outer shell of the reactor body is made of stainless steel. The inner shell of the reactor body is made of Teflon, because of its low thermal conductivity. The air enters the reactor from the top side and leaves the reactor at the bottom. The positions of the 17 thermocouples attached to the reactor are shown in Fig. 2. T_{IN} and T_{OUT} measure the inlet and outlet temperature, respectively. Three sets of thermocouples are labeled as M, B and W, which are located in the middle of the bed, at the inner side of the reactor wall and at the outer side of the body of the reactor, respectively; and in each set, thermocouples are located at five different heights (9, 7, 5, 3 and 1 cm from the bottom of the bed) labeled from 1 to 5.

In the third section, the temperature and humidity of the outflow are measured. The water content in the outflow of the reactor is monitored by a relative humidity/temperature sensor. Based on the measured temperature and relative humidity, the water content in the outflow can be calculated. Since large errors in the absolute humidity can occur measuring at high temperatures (because a high temperature leads to a low relative humidity and therefore a large relative error in the relative humidity), the humidity/temperature sensor is positioned after a chiller. This chiller cools down the outflow, leading to a rise in the relative humidity and therefore the absolute humidity can be determined more accurately.

3. Mathematical model

A non-isothermal and non-adiabatic model including mass and energy transfer equations is developed, to study the thermal dynamics of the system. In this section, the heat and mass balances used in the model are set first. Then the Linear Driving Force (LDF) kinetics model and its coefficient values are explained. Finally, the

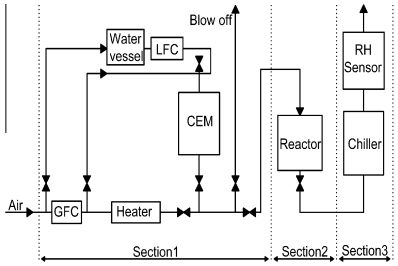

Fig. 1. Schematic view of the components of the system, divided into three sections: flow preparation (1), reactor (2) and outflow measurement section (3).

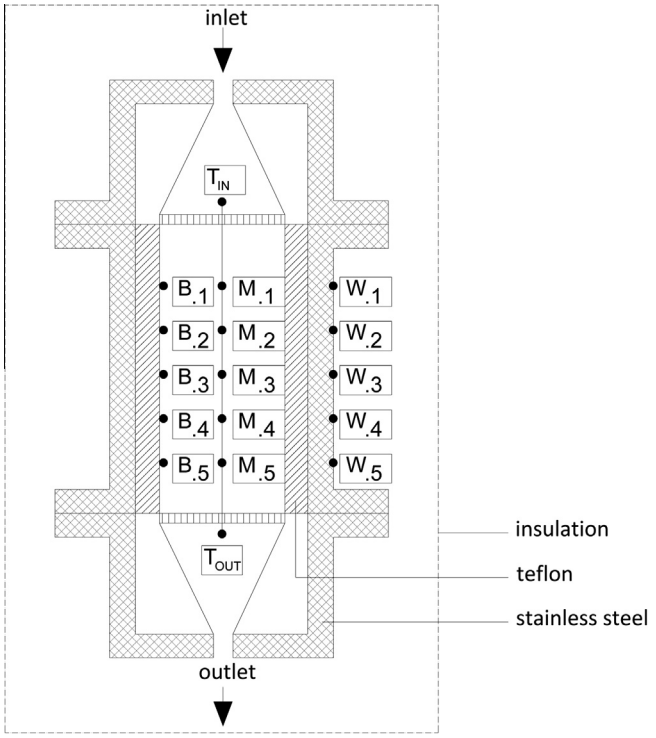

Fig. 2. Position of the thermocouples located at five different heights (1–5) and in the middle of the bed (M), inside wall of reactor body (B) and outside wall (W).

equilibrium isotherms are obtained from experimental results for zeolite 13X adsorption presented by manufacturer.

3.1. Mass and heat balances

The equations in the model which describe the dynamics of the system are formulated under the following assumptions: (a) the flow in the reactor can be described by an axially dispersed plug flow model [25]; (b) heat transfer in radial direction through the bed and the reactor walls can be modeled as a one-dimensional resistance model; (c) the gas phase behaves as an ideal gas and is in thermal equilibrium with the solid phase; (d) the adsorbent beads have identical characterizations and the bed properties are uniform. The temperature distribution problem is determined by two PDEs, one for the bed temperature (T) and the other one for the wall temperature (T_w), connected by heat resistances. An schematic view of the model is shown in Fig. 3. The bed and wall temperatures are solved in the nodal points in axial direction and are in contact through the resistances in radial direction.

By considering these assumptions, the governing heat and mass balances can be written by a set of PDEs along the vertical axial coordinate (z) and the time (t). The overall mass balance is expressed based on the air density, ρ_g:

$$\frac{\partial \rho_g}{\partial t} + u\frac{\partial \rho_g}{\partial z} = 0 \tag{1}$$

where u is the velocity.

The water mass balance is expressed based on the water vapor concentration, c:

$$\frac{\partial c}{\partial t} + u\frac{\partial c}{\partial z} - D_z\frac{\partial^2 c}{\partial z^2} + \frac{(1-\epsilon_b)}{\epsilon_b}\rho_p\frac{dq}{dt} = 0 \tag{2}$$

where ϵ_b is the bed porosity, ρ_p is the particle density, q is the averaged amount of adsorbed water per kg of zeolite and D_z the axial dispersion coefficient which can be derived from Gunn's correlation [25].

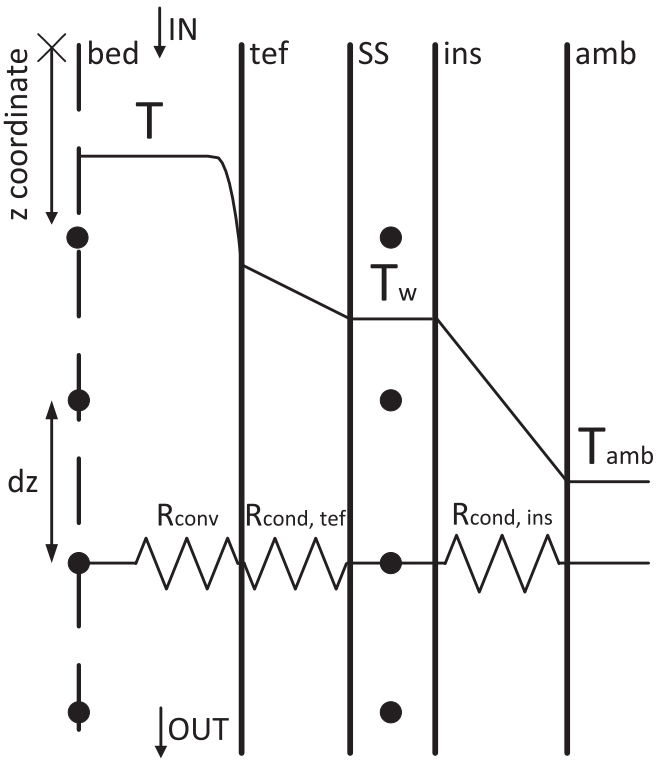

Fig. 3. The temperature distribution problem is determined by two PDEs for the bed temperature T and the wall temperature T_w connected by heat resistances.

The energy balance in the bed is given by:

$$\overline{\rho C_P}\frac{\partial T}{\partial t} + \epsilon_b\rho_g C_{P,g}u\frac{\partial T}{\partial z} - \lambda_z\frac{\partial^2 T}{\partial z^2} - (1-\epsilon_b)\rho_p\frac{dq}{dt}\Delta H + \frac{4}{\pi d_i^2}\frac{(T-T_w)}{R_i} = 0 \tag{3}$$

The effective thermal conductivity in axial direction, λ_z, can be estimated by the model of Zehner and Schlünder [26] which is satisfactory over a broad range of solid-to-fluid thermal conductivities and solid fractions. The overall volumetric heat capacity, $\overline{\rho C_P}$, consists of several terms as shown in Eq. (4), which are the heat capacity of the air in the bed voids (first term), the heat capacity of the air in the beads pores (second term), the heat capacity of the solid (third term) and the heat capacity of the adsorbed water (fourth term). It is dominated by the third and forth terms because of the higher density of the solid phase compared to the gas phase.

$$\overline{\rho C_P} = \epsilon_b\rho_g C_{P,g} + (1-\epsilon_b)\epsilon_p\rho_g C_{P,g} + (1-\epsilon_b)\rho_p C_{P,p} + (1-\epsilon_b)\rho_p q C_{P,v} M_v \tag{4}$$

In Eq. (3), the last term represents the heat loss from the inside reactor wall, at inner diameter of the reactor d_i, per unit of reactor volume. The heat loss through the reactor wall is modeled by considering wall temperature (T_w) and the thermal mass of the reactor wall in another energy balance for the reactor wall:

$$\rho_w C_{P,w}\frac{\partial T_w}{\partial t} - \lambda_{SS}\frac{\partial^2 T_w}{\partial z^2} = \frac{(T-T_w)}{R_i A_w} - \frac{(T_w - T_{amb})}{R_o A_w} \tag{5}$$

in which d_i and d_o refer to the inner and outer diameters of the reactor, R_i and R_o represent the heat resistances at the inner and outer sides of the wall, and A_w is the cross-sectional area of the body of the reactor wall. The heat resistance at the inner side of the wall (R_i) is a summation of the convective heat resistance at the inside wall and the conductive heat resistance in the Teflon layer ($R_i = R_{cond,tef} + R_{conv}$), see Fig. 3. According to Ahn et al. [27] considering heat transfer in a packed bed, the relation between the Nusselt and Reynolds number is assumed to be similar as the case of heat transfer of flow in a circular tube. In this model, the convective heat resistance at the inside wall is calculated using the Nusselt number relation presented in Eq. (6):

$$Nu_{PM} = 0.309 Re_{PM}^{0.8} Pr \tag{6}$$

where the Reynolds number in the porous media is defined as ($Re_{PM} = d_p u\rho_g/\mu_g(1-\epsilon_b)$) and Pr is the Prandtl number. The heat resistance at the outer side of the wall (R_o) is mainly determined by the conductive heat resistance of the insulation layer, and the convective heat resistance at the outside surface of the insulation layer is neglected ($R_o = R_{cond,ins}$), see Fig. 3.

3.2. Kinetics model

The rigorous Chemical Potential Driving Force (CPDF) models, such as the Fickian Diffusion (FD) model, are often used for analyzing adsorbate transport within an adsorbent particle in order to estimate a diffusivity parameter. The characteristics of such models describing the local rates of adsorption at the particle level are often lost during up-scaling to process level. The Linear Driving Force (LDF) model with a lumped mass transfer coefficient, on the other hand, is frequently used for practical analysis of dynamics of the adsorptive processes; because it is simple, analytical, and physically consistent [28]. For many adsorption systems, the diffusion-controlled kinetics may be satisfactory represented by the LDF approximation, first introduced by Glueckauf [29]:

$$\frac{dq}{dt} = k_{LDF}(q_{eq} - q) \tag{7}$$

where q and q_{eq} are the adsorbed and equilibrium loading of water in solid phase per kilograms of dry zeolite, and k_{LDF} is the LDF kinetics coefficient. In real adsorption systems, several mass transfer resistances affect the overall kinetics. The resulting kinetics coefficient k_{LDF} [1/s] is a lumped parameter that considers the external film resistance, the macropore resistance and the micropore resistance [30]:

$$k_{LDF} = \left(\frac{d_p}{6k_f} + \frac{d_p^2}{60\epsilon_b D_P}\right)^{-1} \tag{8}$$

The first term on the right hand side represents the mass transfer resistance in the external film of fluid around the particle. Here, k_f, can be obtained from the Sherwood number expressed by Wakao and Funazkri in the range of Reynolds numbers from about 3 to 10,000 [31]. However the dominant mass transfer resistance for the water vapor adsorption of zeolite 13X is the macropore diffusion resistance [30] presented by the second term on the right hand side of the equation above, in which D_P is given by [32]:

$$D_P = \frac{1}{\tau}\left(\frac{1}{D_M} + \frac{1}{D_K}\right)^{-1} \tag{9}$$

where τ is tortuosity, and D_P, D_M and D_K are the macropore, molecular and Knudsen diffusivity, respectively. The molecular diffusivity for the binary gas mixture of air and water can be evaluated by Chapman–Enskog theory [33], and the Knudsen diffusion by the kinetic theory [32].

The above mentioned kinetics coefficient k_{LDF} is usually only temperature dependent, however in some types of zeolite it is also concentration dependent [34]. As with the zeolite systems the concentration dependency of the kinetics arises mainly from the thermodynamic correction factor; calculations by the corrected coefficient lead to better results [30]:

$$k^*_{LDF} = k_{LDF}\left(\frac{\rho_p RT}{\epsilon_p}\frac{\partial q_{eq}}{\partial p_v}\right)^{-1} \tag{10}$$

3.3. Isotherm models

The water uptake on zeolite 13XBFK (CWK Chemiewerk Bad Kstritz GmbH) is studied, in which BF stands for Binder Free; increasing the amount of active material relative to 13X with binder. Based on BDDT (Brunauer, Deming, Denting, Teller) classification, five isotherm shapes were identified for adsorption in solids [35]. The adsorption of water vapor on zeolite 13X at low water vapor pressure behaves as type 1 [36], where the equilibrium loading of water in the adsorbed phase on zeolite, q_{eq}, is an exponential faction of the water concentration in the gas phase. It can be expressed with the Langmuir or Langmuir–Freundlich isotherms:

$$q_{eq} = \frac{q_{max}(bp_v)^{1/n}}{1 + (bp_v)^{1/n}} \tag{11}$$

where q_{max} is the maximum amount of adsorbed water in high water vapor pressures, p_v is the partial pressure of water vapor, and b and n are temperature-dependent parameters, which can be described as follows [37]:

$$b = b_0 \exp\left(\frac{\Delta E}{RT_0}(T_0/T - 1)\right) \tag{12}$$

$$\frac{1}{n} = \frac{1}{n_0} + \alpha(1 - T_0/T) \tag{13}$$

where T_0 is the reference temperature (that is assumed to be 273.15 K in this work), and b_0 and n_0 are the adsorption affinity constant and exponent constant at reference temperature, respectively. ΔE is the activation energy for desorption.

Experimental information about the water uptake on zeolite 13XBFK is provided by the manufacturer at temperatures of 25, 80 and 95 °C. The Langmuir and Langmuir–Freundlich equations are fitted to the experimental data and the model parameters are extracted. Results are presented in Table 1. Mette et al. [20] approximated the adsorption equilibrium water loading using the Dubinin–Astakhov equation which is based on the micropore filling theory of Polanyi [38]. The comparison between the experimental data, Langmuir–Freundlich and Dubinin–Astakhov fit is shown in Fig. 4. The isotherm model with the obtained fitting parameters is generalized for all the temperatures and is implemented in the model. By using the van't Hoff equation, a concentration dependent form of the isosteric heat of adsorption can be obtained as follows [37]:

$$\Delta H = \Delta E - (\alpha RT_0)n^2 ln\left(\frac{q}{q_{max} - q}\right) \tag{14}$$

In Eq. (14), temperature dependency of the maximum loading (q_{max}) is assumed to be negligible. As shown in Fig. 5, the adsorption heat decreases with water loading. The Langmuir–Freundlich isotherm model, despite having the correct finite capacity at sufficiently large pressures, is applicable only in the intermediate range of water loading ($0 < q < q_{max}$). The physical meaning of ΔE is the isosteric heat of adsorption at the half loading of the material [37].

4. Model validation

The complete model as presented in the former section, is developed and solved in COMSOL Multiphysics, which is a Finite Element Method (FEM) based program. The final set of equations consists of four PDEs:

- Eq. (2) for modeling the water concentration in the gas phase (c);
- Eq. (3) for modeling the bed temperature (T);
- Eq. (5) for modeling the wall temperature (T_w);
- Eq. (7) for modeling the water loading in the solid phase (q).

The PDEs are discretized in space by Lagrange linear shape functions. Both the bed and wall domains are meshed with an element size of 1 mm (chosen based on a mesh convergence study). The solver is a fully coupled time-dependant solver. Backward Differentiation Formula (BDF) scheme (maximum order of 5 and a minimum order of 1) with an initial time step of 0.001 s is used as the time stepping method. The relative, absolute and event tolerances are set to 1E−2. The model is validated by means of comparing the numerically calculated and the experimentally measured temperature profiles, and further by comparison between the thermal fluxes calculated by the model and the ones calculated based on the experimental results.

Table 1
Parameters of the Langmuir and Langmuir–Freundlich equilibrium models for adsorption of water vapor on zeolite 13X.

Parameter	Langmuir	Langmuir–Freundlich
q_{max} [mol/kg]	16	19
b_0 [1/Pa]	1.730	4.002
ΔE [J/mol]	51,800	65,572
n_0 [–]	1	2.976
α [–]	0	0.377
R^2 [–]	0.81	0.96

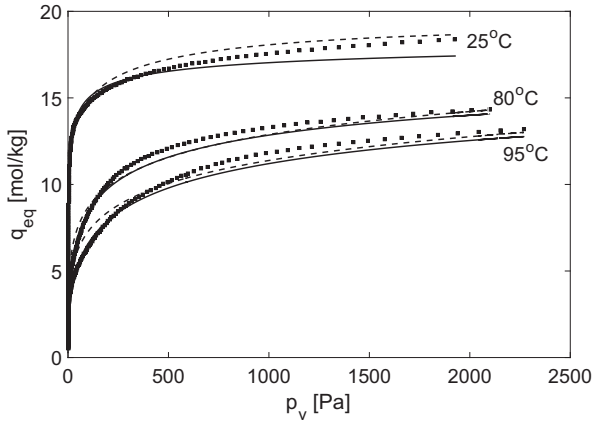

Fig. 4. Langmuir–Freundlich fitted curves (solid lines) on zeolite 13X water uptake experimental data (dots), and Dubinin–Astakhov fitted curves (dash lines).

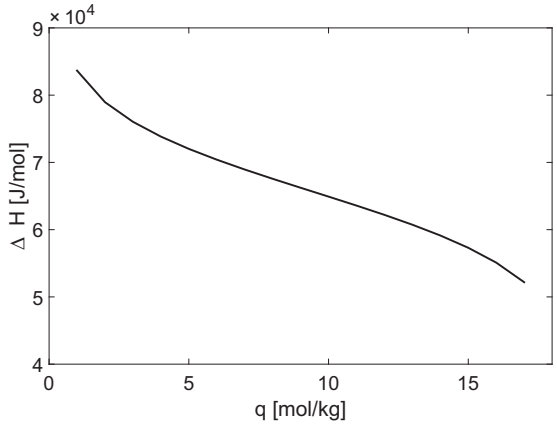

Fig. 5. Isosteric heat of adsorption at different water loadings for zeolite 13XBF.

4.1. Temperature profiles

By introducing the moist air to the packed zeolite as TCM in the reactor, the discharging (hydration) process of the material occurs, which is experimentally performed in the lab-scale setup and numerically simulated by the model. The humidity (water concentration) and flow rate of the inflow moist air are set by the two flow controllers (called as LFC and GFC in Fig. 1). The temperatures during the process time are measured and calculated for different heights in the bed, corresponding to the locations of the thermocouples in the experimental setup (Fig. 2). Properties of the adsorbent zeolite 13X, characteristics of the reactor, and the operational conditions of the adsorption experiment are listed in Table 2.

Table 2
Properties of the adsorbent zeolite 13X, characteristics of the reactor and operational conditions.

Property	Value
Bed porosity (ϵ_b)	0.35
Particle density (ρ_p)	1152 kg/m^3
Particle heat capacity ($C_{P,p}$)	880 J/kg K [20]
Bed height (L)	0.11 m
Reactor inner diameter (d_i)	0.07 m
Reactor outer diameter (d_o)	0.08 m
Wall heat capacity ($\rho_w C_{P,w}$)	3064 kJ/m^3 K
Insulation thickness	0.03 m
Air flow rate	1 l/s
inlet water concentration (c_{in})	0.3 mol/m^3
Ambient temperature	21.5 °C

The experimental results, presented in Fig. 6, show the inlet and outlet temperatures (T_{IN} and T_{OUT}), and the temperatures at five different heights of the bed (M1, M2, M3, M4 and M5). The temperature of the bed increases immediately after the start of the experiment because of the reaction in the bed near the inlet section. The heat is convected to the downstream sections by means of the flow through the bed. Hence the temperature is increased all over the bed. The inlet temperature T_{IN} gradually drops at the beginning of the experiment since the temperature in the humidifier (CEM unit in Fig. 1) drops due to the evaporation energy extracted from it. Since the reaction causes an almost fixed temperature step in the bed, a higher inlet temperature will results in higher bed and outlet temperatures. So the slightly higher temperature at the inlet at the start of the experiment is the reason for the corresponding initial peaks in the temperature of the bed and the outlet air. During this peak, the outlet temperature T_{OUT} is slightly lower than the bed temperature, which is caused by the heat loss to the reactor wall. While the wall temperature increases over time, the heat transfer to the wall decreases due to the heating up the wall and the outflow temperature becomes equal to the bed temperature. After the material at a certain position in the bed is completely hydrated and the reaction is finished, the temperature at the corresponding location in the reactor drops to the cold air inflow temperature. The reaction front passes along the height of the bed and the temperature at each height (at thermocouples M1–5) drops when the reactive zone is passed. The temperature at the outlet of the reactor, T_{OUT}, remains high, because of the reaction heat releasing in the reactive zone which is moving through the bed during time. This process continues until almost 15,000 s when the reaction is finished everywhere in the bed.

The numerically calculated and experimentally measured temperatures at five different heights in the bed (M1–5) are compared in Fig. 7. The comparison of bed temperatures shows good agreement. The calculated wall temperatures in the model are compared to the experimentally measured temperatures at five different heights (W1–5) in Fig. 8. The calculated wall temperatures show a faster increase and decrease and higher maximum than the measured ones. That is probably because of over estimation of the heat transfer coefficient at the inside wall of the reactor in the model. A lower heat transfer between the bed and the wall can also explain the slightly slower decrease in the bed temperature calculated by the model at the end of the cool down process at each height, since the wall looses its heat to the airflow more slowly than calculated.

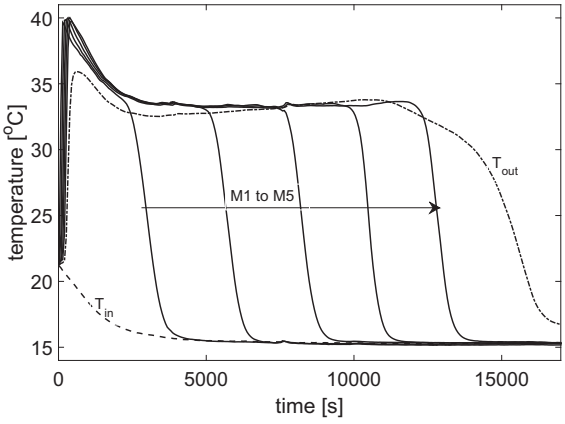

Fig. 6. Temperatures measured at thermocouples T and M, for the experiment with operational conditions mentioned in Table 2.

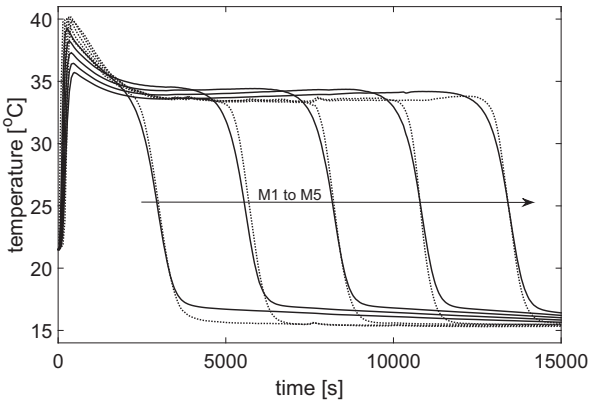

Fig. 7. The numerical (solid) and experimental (doted) bed temperature at thermocouples M1–5, for the experiment with operational conditions mentioned in Table 2.

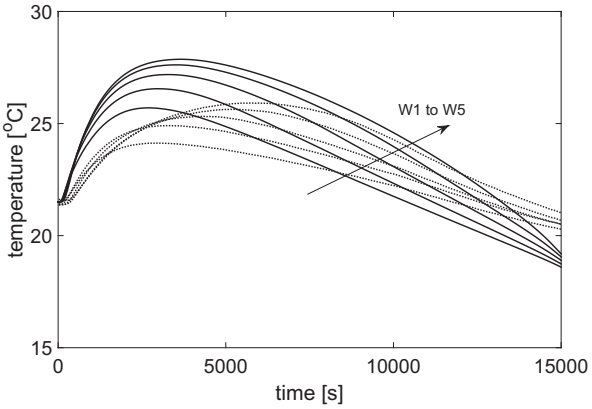

Fig. 8. The numerical (solid) and experimental (doted) reactor wall temperature at thermocouples W1–5, for the operational conditions mentioned in Table 2.

4.2. Isotherm models and kinetics coefficients

Several simulations are run with different equilibrium fits and kinetics coefficients, in order to investigate the influence of the kinetic models and parameters on the results. The temperatures calculated and measured in the middle of the bed at the third thermocouple (M3) are compared, since the temperature profiles at the other thermocouples show the same trend. In Fig. 9, the results from the model with Langmuir–Freundlich and Langmuir adsorption isotherms, using the parameters in Table 1, are compared with the experimental results. The Langmuir–Freundlich isotherm shows a better prediction of the temperature in the reactor than the Langmuir isotherm, which is expected according to the higher accuracy of the Langmuir–Freundlich fit.

The effect of the kinetics coefficient in the LDF model of the adsorption reaction between gas and solid phases (k_{LDF}) on the temperature profile in the reactor is investigated, and the result at the position of the thermocouple M3 is presented in Fig. 10. By increasing the kinetics coefficient, the temperature drop becomes steeper (a sharper reaction interface). The best result is obtained when the kinetics coefficient is around 10×10^{-3} [1/s], and it is best formulated by the corrected coefficient (indicated as k^{*}_{LDF}).

4.3. Energy balance

The energy flows which contribute to the heat balance are shown in Fig. 11. The energy produced during the adsorption ($\dot{Q}_{reaction}$) is partly consumed to heat up the material inside the reactor itself ($\dot{Q}_{sensible}$), and the rest leaves the reactor by means of air flow through the reactor ($\dot{Q}_{convection}$) or is lost from the bed to the reactor body ($\dot{Q}_{loss}$). The net energy (*error*) theoretically should be zero, thus the heat balance is:

$$error = \dot{Q}_{convection} - \dot{Q}_{reaction} + \dot{Q}_{sensible} + \dot{Q}_{loss} \quad (15)$$

The abovementioned energy flows can be calculated by the equations presented in Table 3 for the experimental and numerical results. The convection term (first term in Table 3) in the reactor is calculated as the difference between the convective heat transfer by the outflow and inflow air, which are calculated based on the flow rate and the temperature of the outlet (T_{out}) and inlet (T_{in}) of the reactor (second and third terms in Table 3), respectively. The thermal power produced by the reaction (fourth term in Table 3) is calculated, based on the experimentally measured mole of water accumulation in the reactor $\left(\frac{\dot{m}_{v,in}-\dot{m}_{v,out}}{M_v}\right)$, and based on the numerically calculated reaction rate $\left(\frac{d\bar{q}}{dt}\right)$ integrated over the whole length of the bed (L). The stored sensible heat in the bed (fifth term in Table 3) is calculated based on the time derivative of the bed temperature integrated over the whole length of the bed. To determine the experimental value of this term, it is assumed that in each of the bed segments ($i = 1$–5) the bed temperature is equal to the measured temperature at the center of the bed by the thermocouples M1–5. The thermal loss power (sixth term in Table 3) is calculated based on the temperature difference between the inside and

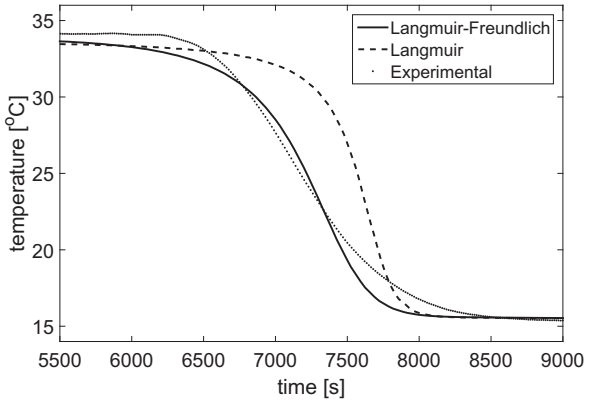

Fig. 9. Effect of the equilibrium fits on the temperature profile at thermocouple M3, for the operational conditions mentioned in Table 2.

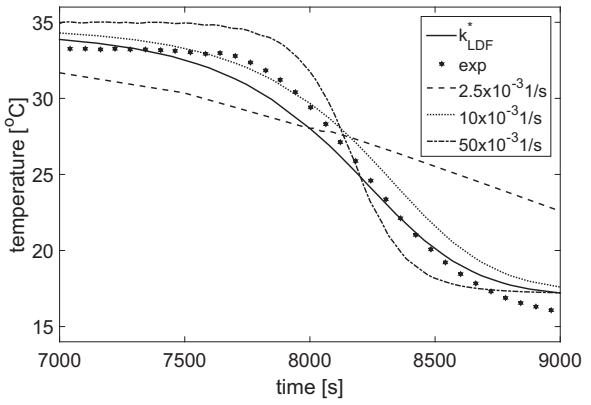

Fig. 10. Effect of the kinetics coefficient on the temperature profile at thermocouple M3, for the operational conditions mentioned in Table 2.

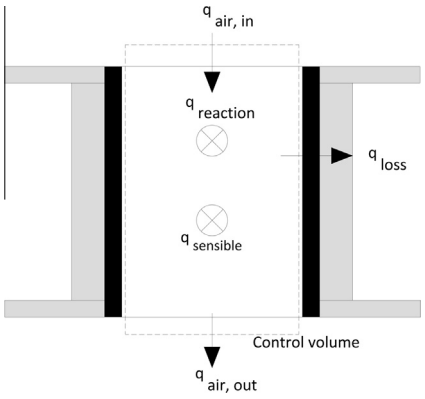

Fig. 11. Schematic view of the energy flows in the reactor.

Table 3
Equations of energy flows in the reactor.

	Term	Experimental	Numerical
1.	$\dot{Q}_{convection}$	$\dot{Q}_{air,out} - \dot{Q}_{air,in}$	$\dot{Q}_{air,out} - \dot{Q}_{air,in}$
2.	$\dot{Q}_{air,out}$	$(\dot{m}_a C_{P,a} + \dot{m}_{v,out} C_{P,v}) T_{out}$	$(\rho_{air} u A_r C_{P,a} + c_{out} M_v u A_r C_{P,v}) T_{out}$
3.	$\dot{Q}_{air,in}$	$(\dot{m}_a C_{P,a} + \dot{m}_{v,in} C_{P,v}) T_{in}$	$(\rho_a C_{P,a} u A_r + c_{in} M_v u A_r C_{P,v}) T_{in}$
4.	$\dot{Q}_{reaction}$	$\frac{\dot{m}_{v,in} - \dot{m}_{v,out}}{M_v} \Delta H$	$\int_0^L \rho_b A_r \Delta H \frac{d\bar{q}}{dt} dz$
5.	$\dot{Q}_{sensible}$	$\sum_{i=1}^{5} \overline{\rho C_P} A_r \frac{\Delta T_{Mi}}{\Delta t} \Delta L$	$\int_0^L \overline{\rho C_P} \frac{dT}{dt} dz$
6.	$\dot{Q}_{loss}$	$\sum_{i=1}^{5} \frac{T_{Bi} - T_{Wi}}{R} \Delta L$	$\int_0^L \frac{T - T_w}{R} dz$

Table 4
Total energies calculated based on experimental and numerical results for hydration.

Term	Experimental	Numerical
$Q_{convection}$ [kJ]	277	270
$Q_{reaction}$ [kJ]	287	295
$Q_{sensible}$ [kJ]	−3	−7
Q_{loss} [kJ]	8	32
error [kJ]	−5	0

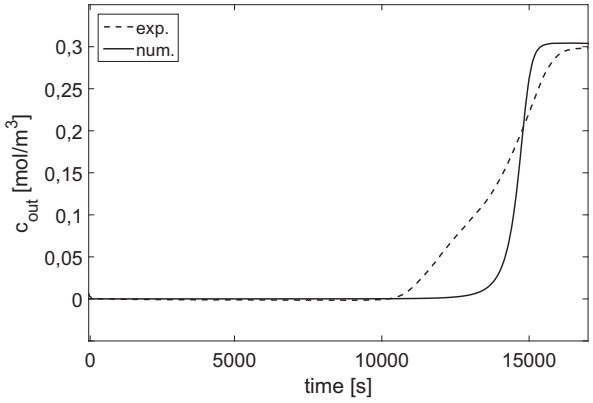

Fig. 13. The numerical and experimental concentrations at the outlet of the reactor, for the operational conditions mentioned in Table 2.

outside wall of the reactor, and the heat resistance of the wall (R) integrated over the whole length of the bed. Calculated heat flows during time based on the numerical and experimental results are shown in Fig. 12. The total produced or consumed powers are integrated during the whole process time and the resulting energies are presented in Table 4.

The heat fluxes, explained in the previous paragraph, are calculated based on both the experimentally measured temperatures and numerically calculated temperatures. As can be seen in Fig. 12, the calculated heat fluxes based on the experimental and numerical results are in good agreement, except for some deviations for the convection and reaction powers at the end of the process. The difference in the reaction power follows the same trend as the difference between calculated and measured water vapor concentrations at the outlet of the reactor (Fig. 13). The water vapor concentration at the outlet of the reactor increases when the bed is fully hydrated and no more water can be adsorbed by

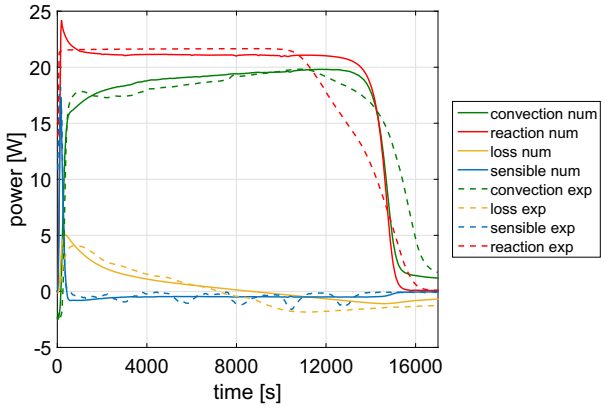

Fig. 12. Numerical (solid) and experimental (dotted) heat fluxes in the reactor during the process time.

the material. The measured water vapor concentration increases slower compared to the simulated one. This slower increase does not seem to be related to any limitation in the kinetics of the zeolite, since the decline in temperature after passing of the thermal front is very rapid, as shown in Fig. 6. Possibly, this effect may be related to a faster completion of the reaction in the near wall region than in the center of the reactor allowing vapor to pass in the near-wall region, while the reaction in the center is still ongoing. This could be caused by several effects, such as e.g. non-uniform flow due to higher porosity near the wall, or due to less effective drying of the zeolite during the charging state due to heat losses at the wall. The model, with the assumption of one dimensionality, is not able to determine the significance of these effects and validity of these hypotheses. It suggests that for better understanding of heat and mass transfer phenomena in radial direction, a more sophisticated investigation on the modeling is needed; however the difference is only seen in the powers at the end of the process, and has only a limited effect on the energy, as the power is overestimated in one part (from around 11,000 s to 15,000 s) and underestimated in another (after 15,000 s).

As can be seen in Fig. 12 and Table 4, the heat loss to the wall based on the numerical results is higher than the one based on the experimental results. Because the heat loss based on the experimentally measured temperatures becomes negative after around 8000 s. It means that the reactor wall releases part of its sensible heat back to the bed instead of losing it to the ambient. For the numerical results, this happens in a later stage of the process. The heat loss predicted by the model in the first phase, when the heat loss is positive and the wall temperature is increasing, is close to the measured value. It suggests that the heat transfer coefficient at the inside wall when the reactor body is releasing heat to the bed should be calculated in a different way than when the heat is transferred from the bed to the wall. In this specific condition, the heat loss and the sensible heat stored in the bed are negligible compared to the reaction heat and the convection heat transfer by the air flow. That is because the sensible heat stored in the bed and most of the heat loss from the bed to the wall are released again to

the air in a later phase of the process. It happens when the temperature of the air drops. The calculated sensible heats are negative because the starting bed temperature is higher than the inlet temperature at the end of the process (Fig. 6) due to the cooling down of the humidifier by evaporation ($T_{in} < T_{amb}$).

5. Parametric study

In the previous section, the model is validated by the experimental results from the lab-scale reactor with the characteristics presented in Table 2. In this section, the validated model is used to study the effect of different parameters on the performance of an up-scaled reactor with the characteristics presented in Table 5. The effect of the kinetics coefficient and the residence time on thermal performance of a thermochemical heat storage reactor under full scale normal operating conditions is investigated. A segment of a large scale reactor with a segment volume of about 51 l is defined in the model and a larger air flow rate (compared to the lab-scale case) is applied to get a high heating power in the order of 1 kW. The inlet water concentration is chosen at around 13 mbar water vapor pressure (being the vapor pressure at 10 °C, which is a typical borehole temperature in the Dutch climate) [10], and the whole reactor is initially at ambient temperature. The characteristics of this large scale reference case are presented in Table 5.

5.1. Effect of kinetics coefficient

The thermal performance of the reactor for different kinetics coefficients is investigated by introducing the efficiency of the reactor as $\eta = Q_{convection}/Q_{reaction}$ and the average power of the reactor. The results are shown in Figs. 14 and 15, respectively, for three cases where the inlet temperature is set as: (1) the experimentally measured inlet temperature in the lab-scale experiment, (2) ambient temperature, and (3) 40 °C. The first case is the one presented in Fig. 6. The second one is simulating the condition that the humid cold air is warmed up to the ambient temperature before entering the reactor. The third case is resembling the reactor under normal operating conditions for heating purposes in the built environment. In this case, since the achievable temperature step in the reactor by means of the reaction is limited, a heat recovery system should be used to preheat the inflow air of the reactor. This is done by transferring the existing excess of heat in the exhaust air from the system [10].

In Fig. 14 for the first case ($T_{in} = T_{exp}$), it can be seen that the efficiency slightly decreases for larger values of the kinetics coefficient. Caused by the fact that the inlet temperature is lower than the ambient temperature, a higher efficiency is obtained for a slower reaction. It means that at a certain time in parts of the reactor where the reaction is finished, the bed actually gains energy from the ambient, so the efficiency increases by decreasing the kinetics coefficient. By increasing the inlet temperature to the ambient temperature, the change in the efficiency of the reactor for different kinetics coefficients is not significant, because there is no energy gain from the ambient. By further increase in the inlet temperature to 40 °C the efficiency drops further. For this case, the efficiency decreases for lower values of the kinetics coefficient, because for slow reactions, the total process time is larger which leads to a higher heat loss.

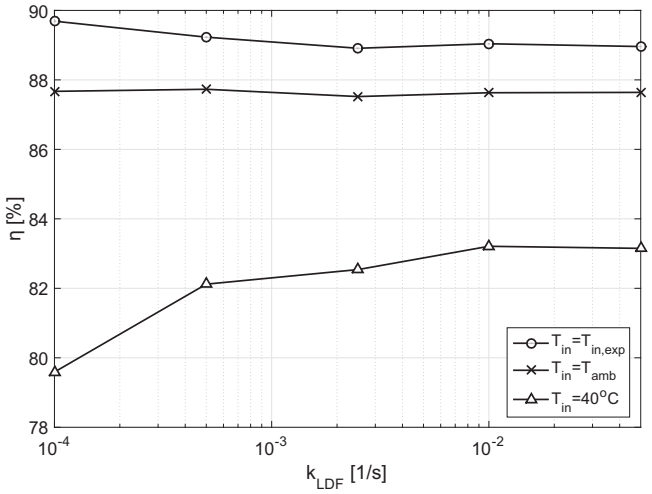

Fig. 14. Effect of kinetics coefficient on efficiency of the reactor with a segment volume of 51 l at different inlet temperatures.

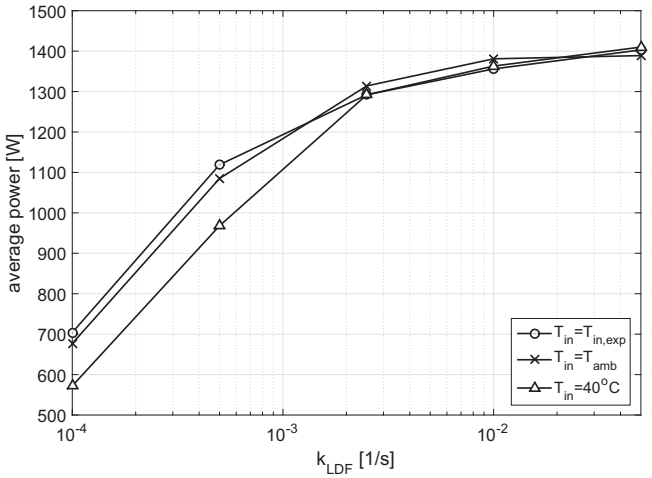

Fig. 15. Effect of kinetics coefficient on average power of the reactor with a segment volume of 51 l at different inlet temperatures.

In Fig. 15, it can be seen that the power is lower for higher inlet temperatures due to the higher heat loss, but for the higher kinetics coefficient this difference is small. The declining trend of the average power by decreasing the kinetics coefficient is similar in all the cases. In addition, the average power decreases for lower values of the kinetics coefficient, which leads to a smaller temperature step. A lower temperature in the reactor leads to a higher water uptake by the zeolite material (Fig. 4), and more adsorption energy is released. Also heat loss decreases because of the smaller temperature gradient over the reactor wall. It can be seen that for the kinetics coefficients larger than around 0.001 [1/s] the efficiency remains in a same range. On the other hand, for faster reaction (higher kinetics coefficient) the total adsorption energy produced is lower because of the lower water uptake at higher temperatures, and the heat loss is larger caused by the larger temperature gradient over the reactor wall. However, the total reaction time is shortened because of the fast reaction. Hence, the change in the total heat loss energy is limited, resulting in almost the same efficiencies for high kinetics coefficients.

Table 5
Characteristics of the large scale reference case.

Property	Value
Bed height (L)	0.56 m
Reactor inner diameter (d_i)	0.34 m
Reactor outer diameter (d_o)	0.35 m
Air flow rate	40 l/s
Inlet water concentration (c_{in})	0.57 mol/m^3
Ambient temperature	21.5 °C

5.2. Effect of residence time

A parameter study is carried out into the effect of the gas flow rate on thermal performance of a thermochemical heat storage reactor under full scale normal operating conditions. The same reactor as in the previous section is considered (Table 5) and the results are presented in Fig. 16. The efficiency of the reactor in all the cases increases by increasing the gas flow rate to around 80 l/s. By further increasing the gas flow rate for the cases with inlet temperature the same as in the lab-scale experiment and with the inflow at ambient temperature, the efficiency stays the same. However, the efficiency decreases for high volumetric flows for the case with the inlet temperature at 40 °C. An optimum flow rate of around 80 l/s can be seen for this case.

In order to investigate the effect of the gas flow rate on the performance of reactors with different sizes, the residence time of the gas flow in the reactor is defined as the reactor volume divided by the gas flow rate. The efficiencies of reactors with different sizes for different residence times are shown in Fig. 17. In all cases the aspect ratio of the reactor is constant ($L/d_i = 1.65$). By increasing the size of the reactor, the efficiency generally increases. For each reactor size, there is an optimum residence time (around 0.6–0.7 s), which corresponds to an optimum flow rate. The optimum flow rate for each reactor size is shown in Fig. 18, and the optimum residence time is found to be 0.62 s.

The effect of the kinetics coefficient on the efficiency of a reactor with a volume of 51 l is investigated (Fig. 19). By decreasing the kinetics coefficient, the efficiency of the reactor generally decreases. The optimum efficiency of the reactor (at the optimum residence time) drops from around 84% for the kinetics coefficient of 100×10^{-4} to around 53% for the kinetics coefficient of 0.10×10^{-4}. In addition, the curves get flatter for lower kinetics coefficients, which means that the efficiency of the reactor is less sensitive to the residence time change. In other words, the performance of a thermochemical reactor is limited by the kinetics for the case of a slow reaction, and by the flow rate for the case of a fast reaction. It can be seen in Fig. 20, where each point represents the optimum efficiency of a reactor (with volume of 51 l) working with the correspondent kinetics coefficient. The points are fitted with a linear function to the inverse of the kinetics coefficient. For smaller kinetics coefficient (slower reaction), in the right hand side of the graph, the optimum residence time is larger, because the water vapor in the flow needs more time to be adsorbed by

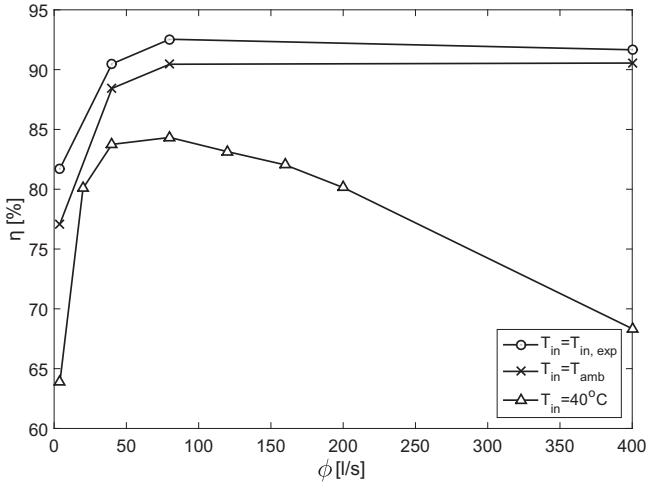

Fig. 16. Effect of gas flow rate on efficiency of the reactor with a segment volume of 51 l at different inlet temperatures.

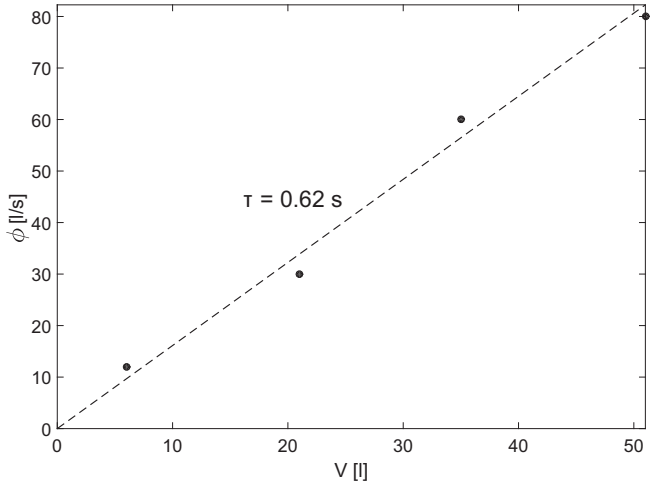

Fig. 18. Optimum residence time for different reactor volumes with the inlet temperature at 40 °C (the kinetics coefficient is calculated by Eq. (10)).

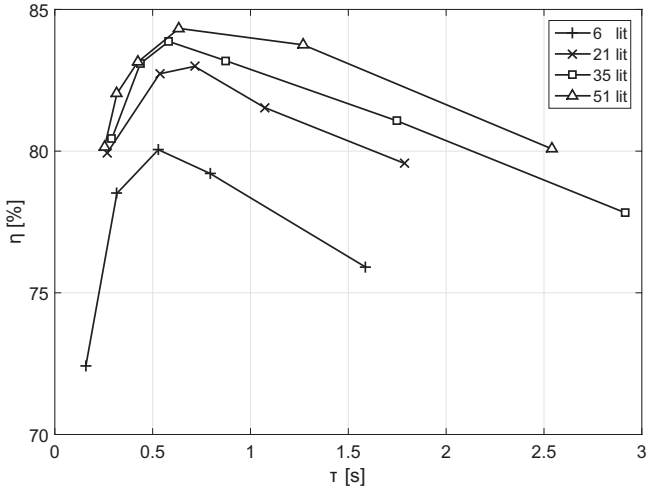

Fig. 17. Effect of gas residence time in the reactor on efficiency of the reactor for the different reactor volumes with the inlet temperature at 40 °C (the kinetics coefficient is calculated by Eq. (10)).

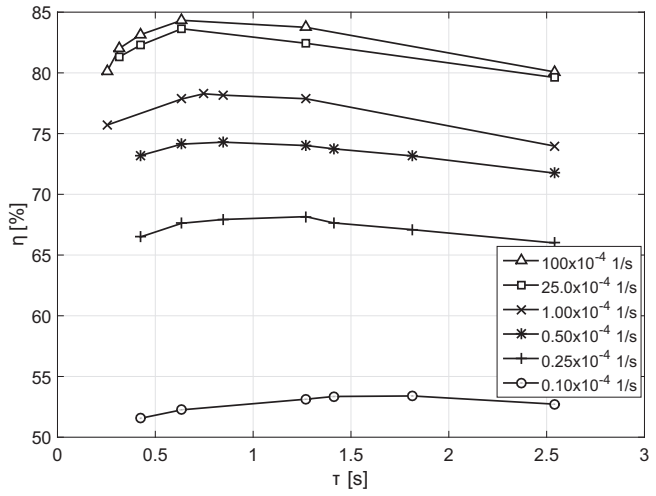

Fig. 19. Effect of gas residence time on the efficiency of the reactor with a segment volume of 51 l and the inlet temperature at 40 °C for different kinetics coefficients.

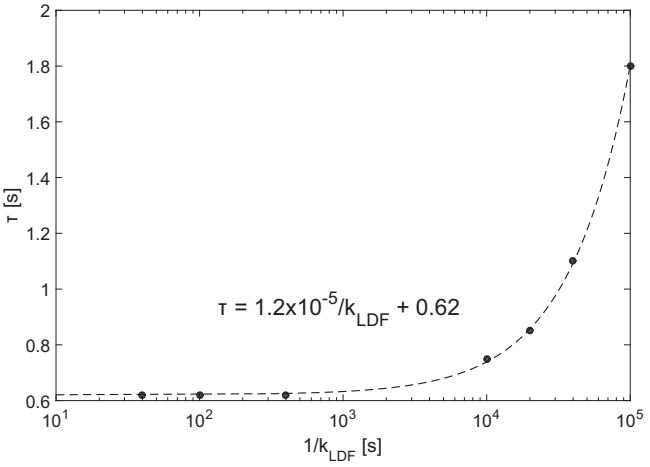

Fig. 20. Optimum flow rate in the reactor with a segment volume of 51 l and the inlet temperature at 40 °C for different kinetics coefficients.

the material. However, for larger values of the kinetics coefficient, in the left hand side of the graph, the optimum residence time is not dependent on the kinetics coefficient but has a constant value of $\tau = 0.62$ s, as shown Fig. 18.

6. Conclusions

A non-isothermal and non-adiabatic model is developed for the thermal dynamics of a fixed-bed reactor filled with zeolite 13X, and experiments are done in a lab-scale reactor setup. The numerically calculated and experimentally measured temperatures are compared and are in a good agreement. The effect of the kinetic parameters on thermal dynamics of the system is investigated. In particular, attention is given to the choice of the isotherm model (Langmuir or Langmuir–Freundlich) and the effect of the kinetics coefficient in the LDF model of the adsorption reaction between gas and solid phases. Based on the comparison between model and experiment, it is found that the Langmuir–Freundlich fit is a better option than a simple Langmuir fit, although using the Langmuir fit makes the simulation slightly faster. The more accurate value of the kinetics coefficient is determined to be the one corrected by the thermodynamics correction factor (presented in Eq. (10)). From this work, predictions of the thermal dynamics in the lab-scale reactor are achieved for the case of water vapor sorption in a zeolite 13X bed. The thermal powers in the reactor are calculated based on the numerical and experimental results and are compared. The model is also validated by comparing the numerically and experimentally determined thermal powers.

The effect of the kinetics coefficient on the efficiency of a large scale reactor is studied. It is found that slower adsorption reduces both the efficiency (from around 83% to around 80%) and the power of the reactor (from around 1.4 kW to around 0.6 kW). However, this effect is only significant below a threshold value of the kinetics coefficient, which for the present case was found to be about 0.001 [1/s]. Above this threshold value, effect of the kinetics coefficient on the efficiency and the power of the reactor is small.

It is found that for each reactor size there is an optimum flow rate. For the present case the residence time of about 0.62 [s] provides the maximum efficiency in a large scale reactor. The optimum residence time (and hence the optimum flow rate) is not dependant on the kinetics coefficient of the reaction for the large values of the kinetics coefficient (for this case, higher than around 0.001 [1/s]). For smaller values of the kinetics coefficient, a further decrease in the kinetics coefficient causes an increase in the optimal residence time.

Since mass and heat transfer are determining phenomena dictating the performance of a reactor, an accurate model describing these phenomena is an indispensable tool to come to an efficient design of a large-scale thermochemical heat storage reactor. This study shows that the heat transfer to the inside wall of the reactor plays an important role in predicting proper values of heat fluxes. Therefore, the model will be improved in a future study by considering the radial heat transfer in a 2D calculation, Which will increase the computational time, but it can be helpful to get more detailed insight. For further studies on a complete thermochemical heat storage system, simple models for other parts of the system can be combined with the presented 1D reactor model. Such a complete model can predict the thermal dynamics of the system and be applied to the energy analysis, design and optimization of a new thermochemical heat storage system.

Acknowledgement

This research has been made possible by the Smart Energy Regions Brabant program, funded by the Province of North-Brabant.

References

[1] Y. Saheb, Modernising Building Energy Codes to Secure our Global Energy Future, The IEA Policy Pathway Series, 2011.
[2] H. Garg, S. Mullick, A. Bhargava, Solar Thermal Energy Storage, 1985, cited By 154. <http://www.scopus.com/inward/record.url?eid=2-s2.0-0022172171&partnerID=40&md5=2b5e7d1e40be632714f2e779cc429f2a>.
[3] P. Tatsidjodoung, N.L. Pierrs, L. Luo, A review of potential materials for thermal energy storage in building applications, Renew. Sustain. Energy Rev. 18 (2013) 327–349, http://dx.doi.org/10.1016/j.rser.2012.10.025. <http://www.sciencedirect.com/science/article/pii/S1364032112005679>.
[4] D. Aydin, S.P. Casey, S. Riffat, The latest advancements on thermochemical heat storage systems, Renew. Sustain. Energy Rev. 41 (2015) 356–367.
[5] H. Zondag, A. Kalbasenka, M. van Essen, L. Bleijendaal, R. Schuitema, W. van Helden, L. Krosse, First studies in reactor concepts for thermochemical storage, in: Proc. Eurosun, 2008.
[6] Alibaba.com. <http://www.alibaba.com/l>.
[7] J. Jänchen, K. Schumann, E. Thrun, A. Brandt, B. Unger, U. Hellwig, Preparation, hydrothermal stability and thermal adsorption storage properties of binderless zeolite beads, Int. J. Low-Carbon Technol. 7 (4) (2012) 275–279.
[8] K.E. NTsoukpoe, H. Liu, N.L. Pierrs, L. Luo, A review on long-term sorption solar energy storage, Renew. Sustain. Energy Rev. 13 (9) (2009) 2385–2396, http://dx.doi.org/10.1016/j.rser.2009.05.008. <http://www.sciencedirect.com/science/article/pii/S1364032109001129>.
[9] B. Mette, H. Kerskes, H. Drück, H. Müller-Steinhagen, New highly efficient regeneration process for thermochemical energy storage, Appl. Energy 109 (2013) 352–359.
[10] H. Zondag, B. Kikkert, S. Smeding, R. de Boer, M. Bakker, Prototype thermochemical heat storage with open reactor system, Appl. Energy 109 (2013) 360–365.
[11] N. Yu, R. Wang, L. Wang, Sorption thermal storage for solar energy, Prog. Energy Combust. Sci. 39 (5) (2013) 489–514.
[12] B. Michel, P. Neveu, N. Mazet, Comparison of closed and open thermochemical processes, for long-term thermal energy storage applications, Energy 72 (2014) 702–716.
[13] B. Zettl, G. Englmair, G. Steinmaurer, Development of a revolving drum reactor for open-sorption heat storage processes, Appl. Therm. Eng. 70 (1) (2014) 42–49.
[14] H. Zondag, R. Schuitema, L. Bleijendaal, J.C. Gores, V. van Essen, W. Van Helden, M. Bakker, R&d of thermochemical reactor concepts to enable seasonal heat storage of solar energy in residential houses, in: ASME 2009 3rd International Conference on Energy Sustainability Collocated with the Heat Transfer and InterPACK09 Conferences, American Society of Mechanical Engineers, 2009, pp. 831–837.
[15] B. Mette, H. Kerskes, H. Drück, Experimental and numerical investigations of different reactor concepts for thermochemical energy storage, Energy Procedia 57 (2014) 2380–2389.
[16] L.Z. Zhang, L. Wang, Effects of coupled heat and mass transfers in adsorbent on the performance of a waste heat adsorption cooling unit, Appl. Therm. Eng. 19 (2) (1999) 195–215.
[17] M. Duquesne, J. Toutain, A. Sempey, S. Ginestet, E.P. del Barrio, Modeling of a nonlinear thermochemical energy storage by adsorption on zeolites, Appl. Therm. Eng. 71 (1) (2014) 469–480.
[18] L. Sun, N.B. Amar, F. Meunier, Numerical study on coupled heat and mass transfers in an absorber with external fluid heating, Heat Recov. Syst. CHP 15 (1) (1995) 19–29.

[19] N.B. Amar, L. Sun, F. Meunier, Numerical analysis of adsorptive temperature wave regenerative heat pump, Appl. Therm. Eng. 16 (5) (1996) 405–418.
[20] B. Mette, H. Kerskes, H. Drück, H. Müller-Steinhagen, Experimental and numerical investigations on the water vapor adsorption isotherms and kinetics of binderless zeolite 13X, Int. J. Heat Mass Transfer 71 (2014) 555–561.
[21] H. Ahn, C.-H. Lee, Effects of capillary condensation on adsorption and thermal desorption dynamics of water in zeolite 13X and layered beds, Chem. Eng. Sci. 59 (13) (2004) 2727–2743.
[22] B. Dawoud, U. Vedder, E.-H. Amer, S. Dunne, Non-isothermal adsorption kinetics of water vapour into a consolidated zeolite layer, Int. J. Heat Mass Transfer 50 (11) (2007) 2190–2199.
[23] S. Sircar, Linear-driving-force model for non-isothermal gas adsorption kinetics, J. Chem. Soc., Faraday Trans. 1: Phys. Chem. Conden. Phases 79 (4) (1983) 785–796.
[24] S. Lan, H. Zondag, A. van Steenhoven, C. Rindt, Kinetic study of the dehydration reaction of lithium sulfate monohydrate crystals using microscopy and modeling, Thermochim. Acta 621 (2015) 44–55.
[25] J. Delgado, A critical review of dispersion in packed beds, Heat Mass Transfer 42 (4) (2006) 279–310.
[26] M. Kandula, On the effective thermal conductivity of porous packed beds with uniform spherical particles, J. Porous Media 14 (10) (2011) 919–926.
[27] H. Ahn, M.-B. Kim, C.-H. Lee, Effects of heat-transfer coefficients on thermal dynamics in a near-adiabatic fixed bed, Sep. Sci. Technol. 39 (11) (2004) 2627–2654.
[28] S. Sircar, J. Hufton, Why does the linear driving force model for adsorption kinetics work?, Adsorption 6 (2) (2000) 137–147
[29] E. Glueckauf, Theory of chromatography. Part 10. Formula for diffusion into spheres and their application to chromatography, Trans. Faraday Soc. 51 (1955) 1540–1551.
[30] D.M. Ruthven, Principles of Adsorption and Adsorption Processes, John Wiley & Sons, 1984.
[31] N. Wakao, T. Funazkri, Effect of fluid dispersion coefficients on particle-to-fluid mass transfer coefficients in packed beds: correlation of Sherwood numbers, Chem. Eng. Sci. 33 (10) (1978) 1375–1384.
[32] W.J. Thomas, B.D. Crittenden, Adsorption Technology and Design, Butterworth-Heinemann, 1998.
[33] S. Chapman, T. Cowling, The Mathematical Theory of Non-uniform Gases: An Account of the Kinetic Theory of Viscosity, Thermal Conduction and Diffusion in Gases, Cambridge University Press, 1970.
[34] J. Crank et al., The Mathematics of Diffusion, vol. 2, Clarendon press Oxford, 1975.
[35] S. Brunauer, L.S. Deming, W.E. Deming, E. Teller, On a theory of the van der waals adsorption of gases, J. Am. Chem. Soc. 62 (7) (1940) 1723–1732.
[36] Y.K. Ryu, S.J. Lee, J.W. Kim, C.-H. Leef, Adsorption equilibrium and kinetics of H_2O on zeolite 13X, Korean J. Chem. Eng. 18 (4) (2001) 525–530.
[37] D.D. Do, Adsorption Analysis, World Scientific, 1998.
[38] B. Bering, M. Dubinin, V. Serpinsky, Theory of volume filling for vapor adsorption, J. Colloid Interface Sci. 21 (4) (1966) 378–393.

ECN
Westerduinweg 3
1755 LE Petten
The Netherlands

P.O. Box 1
1755 LG Petten
The Netherlands

T +31 88 515 4949
F +31 88 515 8338
info@ ecn.nl
www.ecn.nl